Electronic Supplementary Information

Exfoliation of Amorphous Phthalocyanine Conjugated Polymers into Ultrathin Nanosheets for Highly Efficient Oxygen Reduction

Wenping Liu, Chiming Wang, Lijie Zhang, Houhe Pan, Wenbo Liu, Jun Chen, Dongjiang Yang, Yanjuan Xiang, Kang Wang,* Jianzhuang Jiang,* and Xiangdong Yao*

Experimental Section

AFM images were recorded from a Bruker Multimode 8 system with a silicon cantilever by using tapping mode. All AFM images are shown in height mode without any image processing except flatting. Transmission electron microscopy (TEM) was measured by HT7700 electron microscope at 100 KV. HAADF-STEM images and energy dispersive spectros-copy (EDS) mapping images were taken on a JEM-ARM200F electron microscope operated at 200 kV. AC STEM images were collected from TECNAI 12 and probe-corrected JEOL ARM200F with an acceleration voltage of 80 kV. Solid-state UV-Vis diffuse reflectance spectra were recorded on an SHIMADZU UV-2600 spectrophotometer. IR spectra were recorded as KBr pellets using a Bruker Tensor 37 spectrometer with 2 cm^{-1} resolution. X-ray photoelectron spectra (XPS) data were collected from PHI 5300 ESCA System (PerkineElmer, USA). N_2 adsorption-desorption isotherms were measured on a QuadraSorb SI apparatus at 77 K and the surface areas were calculated by the Brunauere Emmette Teller (BET) method. CV, LSV, and RRDE measurements were conducted on the CHI 760E workstation (CH Instruments, Inc.) with a RRDE-3A rotator (ALS Co., Ltd). The typical three-electrode system was employed to evaluate the electrochemical properties of the prepared catalysts. A typical three-electrode system was employed, using a commercial glassy carbon (GC) electrode (4 mm diameter, 0.1256 cm^2) as the working electrode, a platinum wire and Ag/AgCl electrode (in saturated KCl solution) as the counter and reference electrodes, respectively. All potentials were referred to the reversible hydrogen electrode by adding a value of (0.197 + 0.059×pH) V. All the electrochemical tests in this study were conducted at least three

times to ensure the accuracy of the measurement. Besides, the iR correction was applied to get rid of the influence of the Ohmic resistance, and the effect of the double layer capacitance on the ORR performance of the resulting catalysts was eliminated (the corresponding methods were specified in Supporting Information).

Synthesis of FePc-CP-3. FePc-CP-3 was prepared *via* a solid-state chemical reaction method. The mixture of 1,2,4,5-benzenetetranitrile (50 mg, 0.28 mmol) and $FeCl_2$ (17.8 mg, 0.14 mmol) is ground evenly. Then the mixture was heated in a tube furnace in a nitrogen atmosphere. After carrying out the reaction at 250°C for an hour, the mixture was cooled down to room temperature, and then washed with 1 M hydrochloric acid, distilled water, methanol, and dichloromethane. Finally the product was dried at 80°C under vacuum for 12 h to yield FePc-CP-3 as a dark green powder (55mg).

Preparation of FePc-CP NS@G. A designed volume (2.0 mg mL^{-1}) of the exfoliated FePc-CP NSs was added drop by drop into graphene NSs suspension with concentration of 1.0 mg mL^{-1} under continuous stirring for 8 h at 70°C. The flocculated product was separated by centrifugation. The weight ratio of FePc-CP NS and G was controlled as 2:1.

Preparation of CoPc-CP NS@G. A designed volume (2.0 mg mL^{-1}) of the exfoliated FePc-CP NSs was added drop by drop into graphene NSs suspension with concentration of 1.0 mg mL^{-1} under continuous stirring for 8 h at 70°C. The flocculated product was separated by centrifugation. The weight ratio of FePc-CP NS and G was controlled as 2:1.

Preparation of the working electrode: The catalyst-modified working electrode was fabricated by casting an appropriate amount of catalyst ink, which was obtained by ultrasonically dispersing the catalyst (4 mg) into 1.0 mL ethanol containing 0.2 μL 5wt% Nafion Then, 8 μL of the mixture was dropped onto a polished glassy carbon electrode (4 mm in diameter). The loaded electrode was placed in a 60 °C oven for 10 min to dry and then was taken out to cool down before all the tests. The loading amount of each catalyst was kept at 0.25 mg cm^{-2}.

Cyclic voltammetry (CV). Prior to the test, the electrolyte (0.1 M KOH solution) was bubbled with O_2 for at least 30 min to make it saturated with O_2, and a constant oxygen flow was kept during the measurement. The data was recorded at the scan rate of 50 mV s^{-1} under static conditions when the system became stable. For the methanol tolerance test, after injecting 5 % (volume) methanol into the cell, the electrode was rotated for 5 min to ensure the added methanol dispersed homogeneously in the electrolyte, and then the CV measurement was carried out under static conditions again. The resulting data were corrected to remove the iR drop.

Linear sweep voltammetry (LSV) measurement. The rotating speed of the working electrode is increased from 400 to 2500 rpm at the scan rate of 10 mV s^{-1}. The resulting data were corrected to remove the iR drop and the double-layer effect.

Rotating ring-disk electrode (RRDE) measurement. The rotating speed of the working electrode was fixed at 1600 rpm with the scan rate of 10 mV s^{-1} for the RRDE test. The

electron transfer number (n) is calculated *via* the following equation.[S1,S2]

$$n = 4I_d / (I_d + I_r / N) \tag{1}$$

$$\% \, HO^{2-} = 200(I_r / N) / (I_d + I_r / N) \tag{2}$$

Where I_d stands for the disk current, I_r represents the ring current, and N is the current collection efficiency of the Pt ring, which was identified to be 0.43 in 2 mmol L^{-1} K$_3$Fe[CN]$_6$ and 0.1 M KCl solution.

Koutecky-Levich (K-L) plots. The working electrode was scanned cathodically at the rate of 10 mV s^{-1} with the rotation speed from 400 to 2500 rpm. Koutecky-Levich (K-L) plots (J^{-1} *vs* $\omega^{-1/2}$) were analyzed at 0.3–0.6 V. Koutecky-Levich equation:[S3,S4]

$$1/J = 1/J_L + 1/J_K = 1/(B\omega^{1/2}) + 1/J_K \tag{3}$$

$$B = 0.2nFC_0D_0^{2/3}v^{-1/6}; \, J_K = nFkC_0$$

Where J is the measured current density, J_k and J_L are the kinetic and limiting current densities, ω is the angular velocity, n is transferred electron number, F (96485 C mol^{-1}) is the Faraday constant, D_0 is the diffusion coefficient of O$_2$ in 0.1 M KOH (1.9 × 10^{-5} cm^2 s^{-1}), C_0 is the bulk concentration of O$_2$ (1.2 × 10^{-6} mol cm^{-3}), v is the kinetic viscosity of the electrolyte (0.01 cm^2 s^{-1}), and k is the electron-transfer rate constant. The constant 0.2 is adopted when the rotation speed is expressed in rpm.

iR-Correction. The iR correction has been adopted to remove the influence of Ohmic resistance on the ORR measurements. Specifically, the electrochemical alternating current impedance spectroscopy (EIS) was utilized to measure to Ohmic resistance under the ORR conditions. The potentials were calculated *via* the following equation:[S5]

$$E_{\text{iR-corrected}} = E - iR \tag{4}$$

Where i is the current, R is the uncompensated ohmic electrolyte resistance measured *via* high frequency A.C. impedance in O_2-saturated 0.1 M KOH solution, which is around 50 Ω for all the tested samples.

Double-Layer Capacitance Correction. The ORR test was conducted in ultra-high purity nitrogen saturated and oxygen saturated 0.1 M KOH solution, respectively, and the final LSV data was obtained by subtracting the LSV data measured in N_2-saturated 0.1 M KOH solution from the LSV results measured in O_2-saturated 0.1 M KOH solution. All the LSV curves in this work have been corrected by this method.

Mass Activity. The mass activity was obtained by normalizing the kinetic current (I_k) to the electrode mass. I_k is obtained by multiplying J_k (derived from the Koutecky–Levich equation at 0.9 V *vs* RHE) with the geometric area of the glassy carbon disk.

Theoretical Caculation. The interaction between the $4D_{4h}$ model with all the nine structural models fabricated by four phthalocyanine molecules with D_{4h} or D_{2h} symmetry is calculated at the level of M06-2X-D3/6-311+G(d,p). Density functional theory (DFT) calculations for the $Fe_{0.5}Co_{0.5}Pc$-CP NS@G composite were performed on the basis of PBE. A mixed basis set, where Lanl2DZ for Fe/Co and 3-21g for C/N/H, was employed. All calculations were carried out by Gaussian 09 D.01 software package.[S6-S9]

The calculation of turnover frequency (TOF).

The TOF is calculated by following Equations,

$$TOF = \frac{N_{O_2 \ per \ unit \ area}}{N_{active \ site \ per \ unit \ area}} \qquad (5)$$

$$N_{O_2 \ per \ unit \ area} = \frac{j}{4f} \qquad (6)$$

$$N_{active \ site \ per \ unit \ area} = N_{Fe \ and \ Co \ atoms} = \frac{m_{Fe}}{M_{Fe}} + \frac{m_{Co}}{M_{Co}} \qquad (7)$$

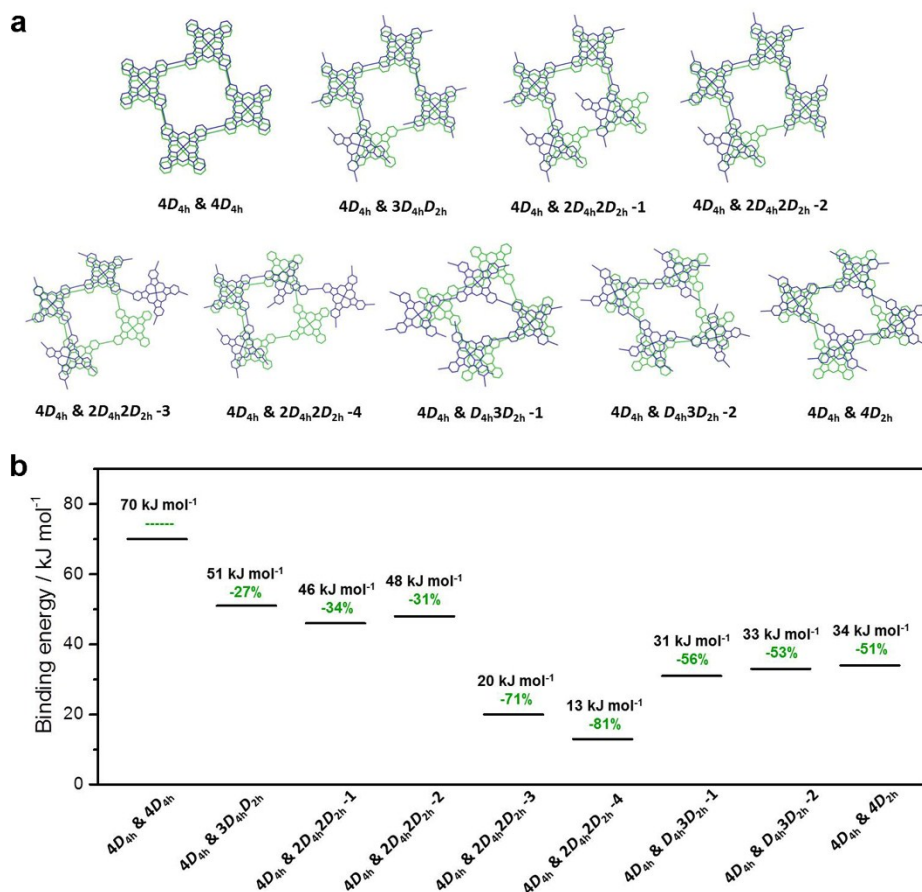The F is Faraday constant, the j is current density, m_{Fe} and m_{Co} are the mass of Fe and Co per unit area and the M_{Fe} and M_{Co} are atomic mass of Fe and Co.

Fig. S1. (a) Schematic diagram for the π-π interactions between the $4D_{4h}$ model (green) with all the nine quadrilateral structural models fabricated by four phthalocyanine molecules with D_{4h} or D_{2h} symmetry (blue) and (b) the corresponding binding energy per phthalocyanine molecule between two models.
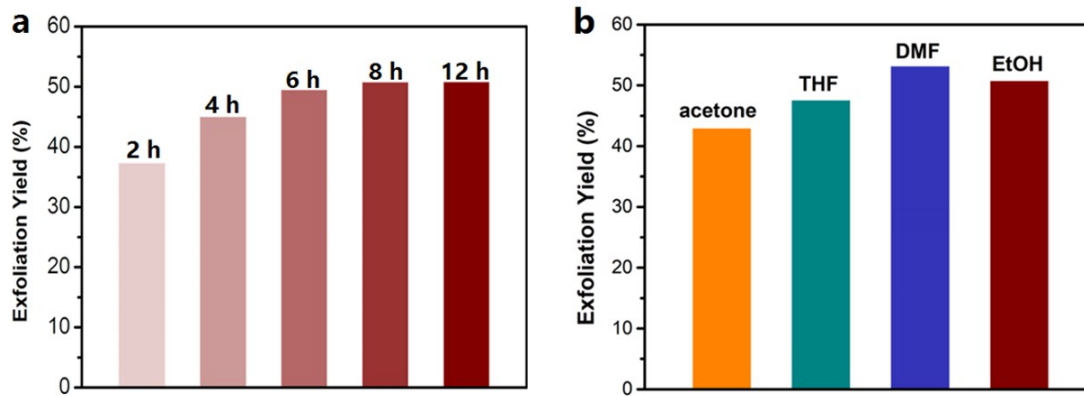
Fig. S2 The ultrasonic exfoliation yield of $Fe_{0.5}Co_{0.5}Pc$-CP NSs (a) in ethanol at different times and (b) in different organic solvents for 8 h.
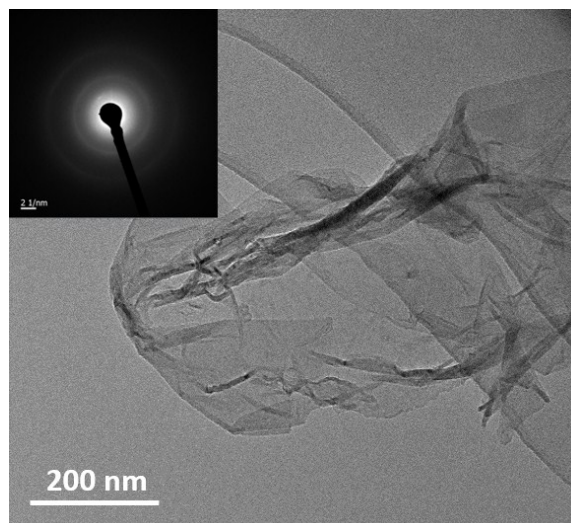
Fig. S3 TEM image and SAED pattern of the $Fe_{0.5}Co_{0.5}Pc$-CP NSs.
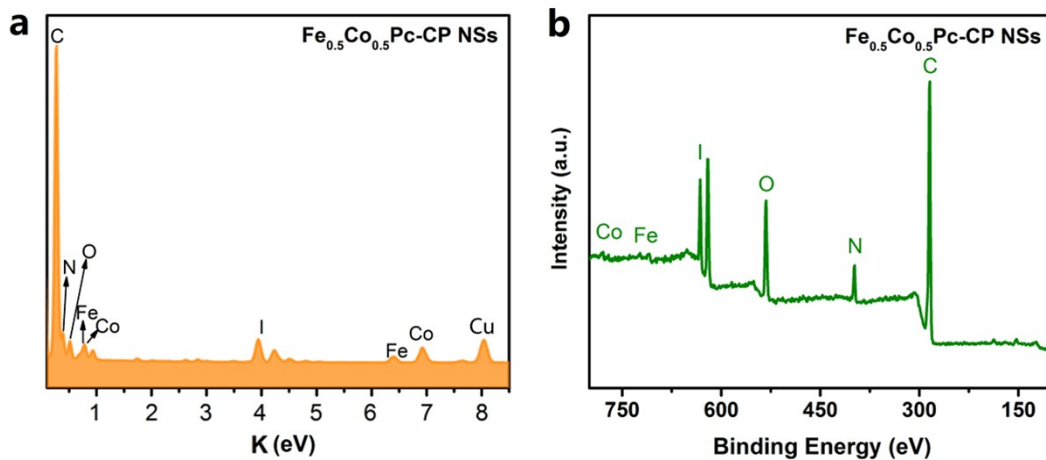
Fig. S4 EDS (a) and XPS overall spectrum (b) of results of the $Fe_{0.5}Co_{0.5}Pc$-CP NSs.
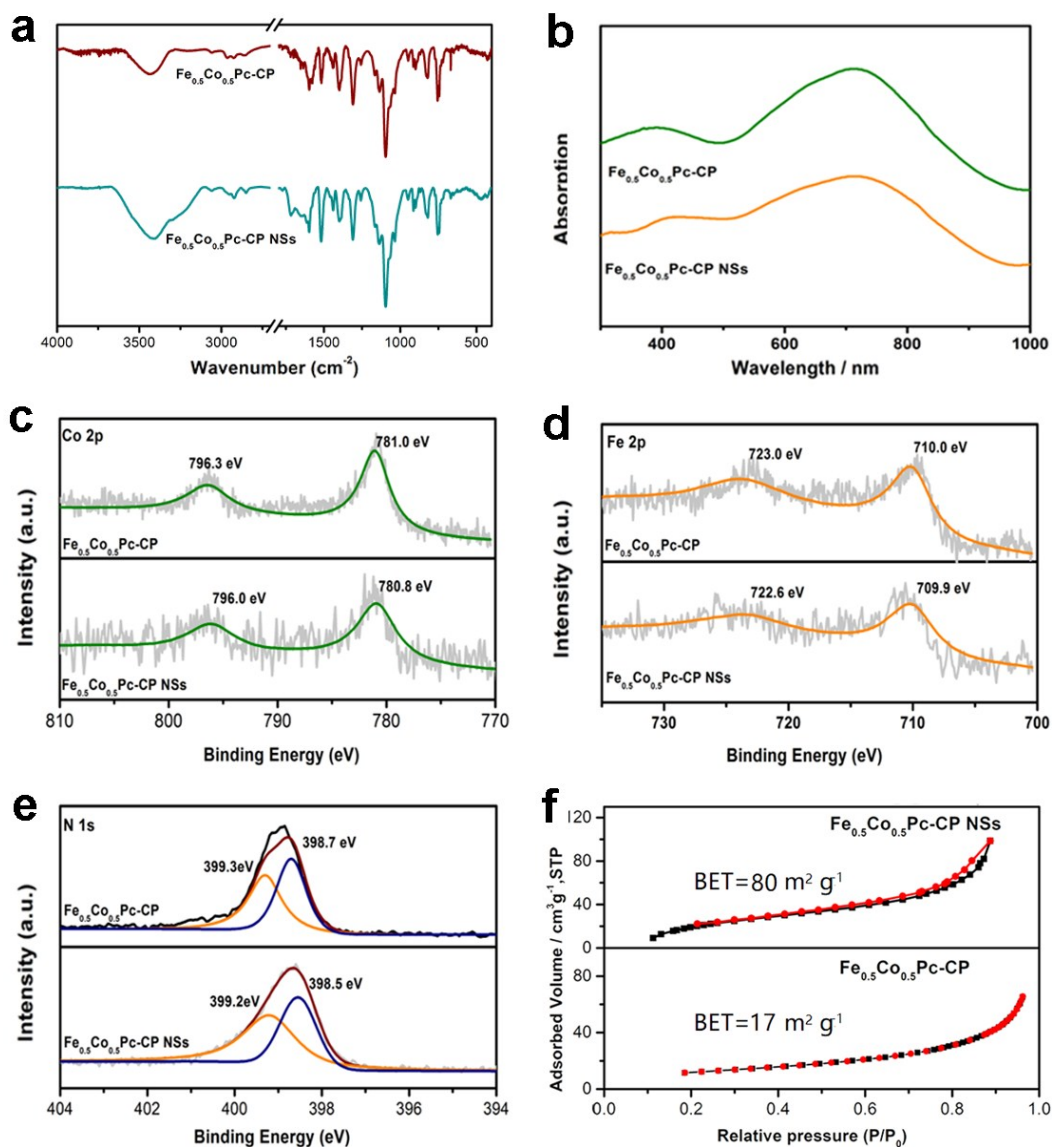
Fig. S5 (a) FT-IR spectra of $Fe_{0.5}Co_{0.5}Pc$-CP and $Fe_{0.5}Co_{0.5}Pc$-CP NSs in the region of 400-4000 cm^{-1}. (b) UV-vis diffuse reflectance spectra of $Fe_{0.5}Co_{0.5}Pc$-CP and $Fe_{0.5}Co_{0.5}Pc$-CP NSs. XPS high resolution (c) Co 2p, (d) Fe 2p and (e) N 1s spectra of $Fe_{0.5}Co_{0.5}Pc$-CP and $Fe_{0.5}Co_{0.5}Pc$-CP NSs. (f) The BET surface area of $Fe_{0.5}Co_{0.5}Pc$-CP and $Fe_{0.5}Co_{0.5}Pc$-CP NSs.
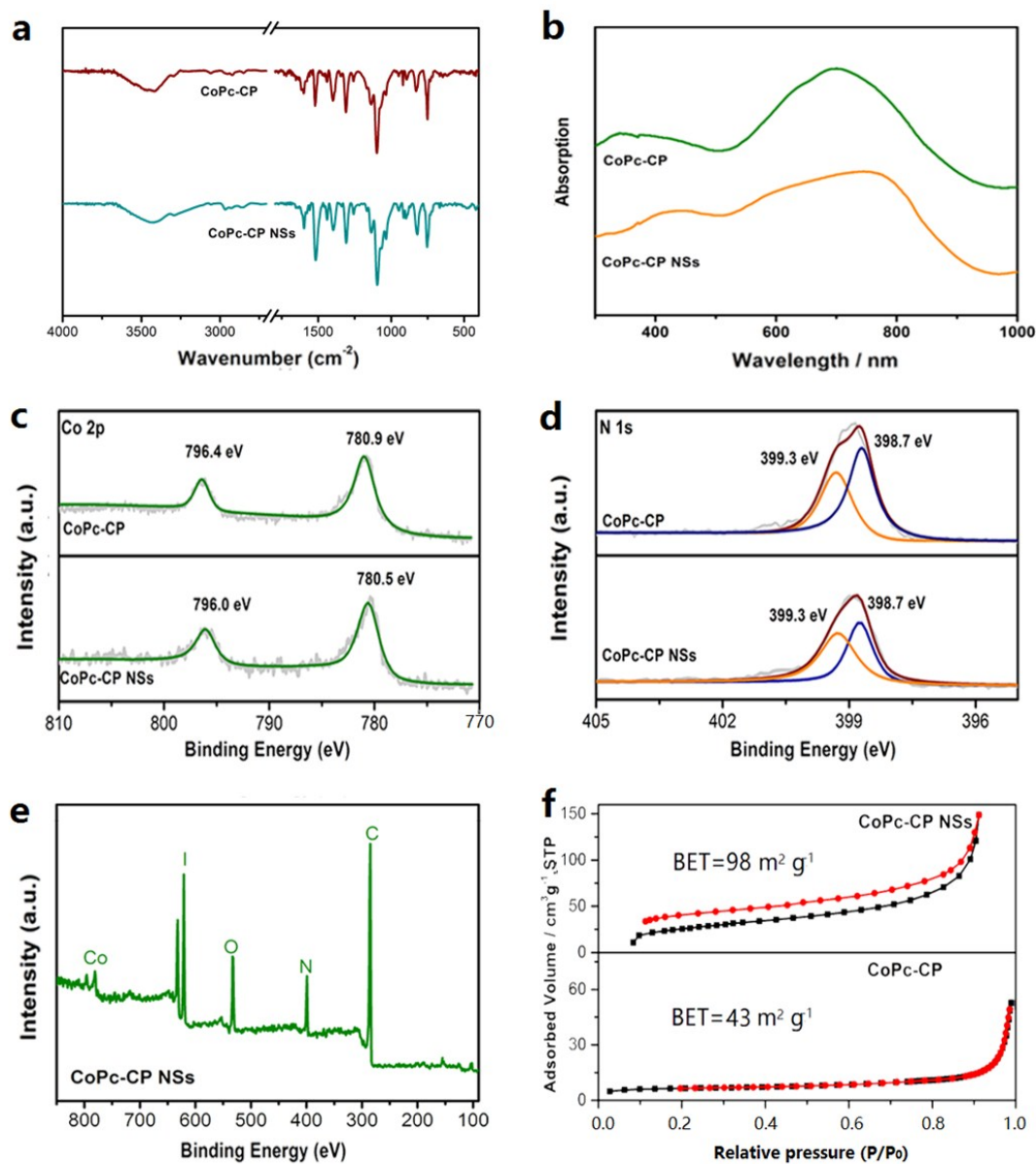
Fig. S6 (a) FT-IR spectra of CoPc-CP and CoPc-CP NSs in the region of 400-4000 cm^{-1}. (b) UV-vis diffuse reflectance spectra of CoPc-CP and CoPc-CP NSs. XPS high resolution (c) Co 2p, (d) N 1s and (e) overall spectra of CoPc-CP and CoPc-CP NSs. (f) The BET surface area of CoPc-CP and CoPc-CP NSs.
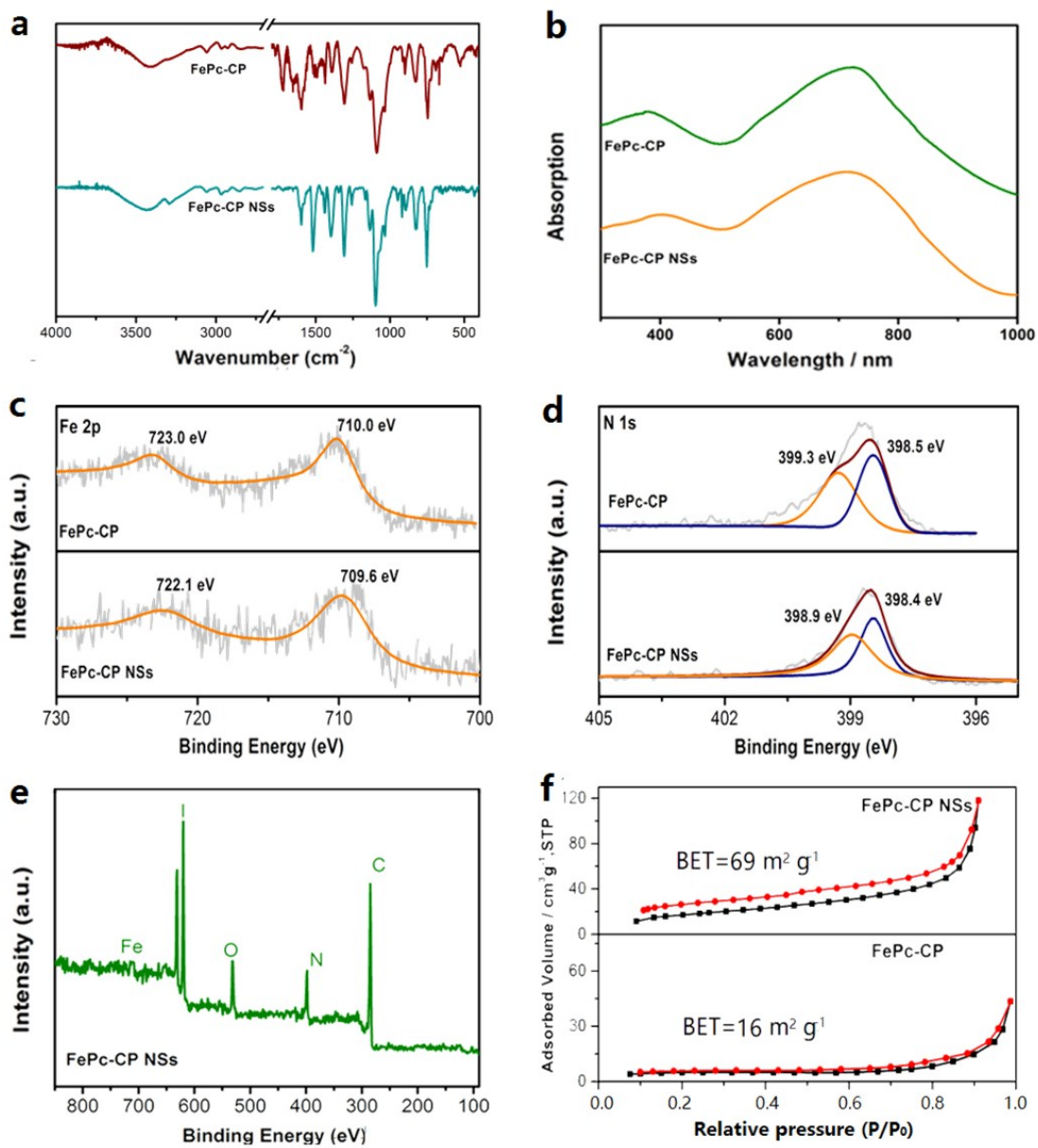
Fig. S7 (a) FT-IR spectra of FePc-CP and FePc-CP NSs in the region of 400-4000 cm^{-1}. (b) UV-vis diffuse reflectance spectra of FePc-CP and FePc-CP NSs. XPS high resolution (c) Fe 2p, (d) N 1s and (e) overall spectra of FePc-CP and FePc-CP NSs. (f) The BET surface area of FePc-CP and FePc-CP NSs.
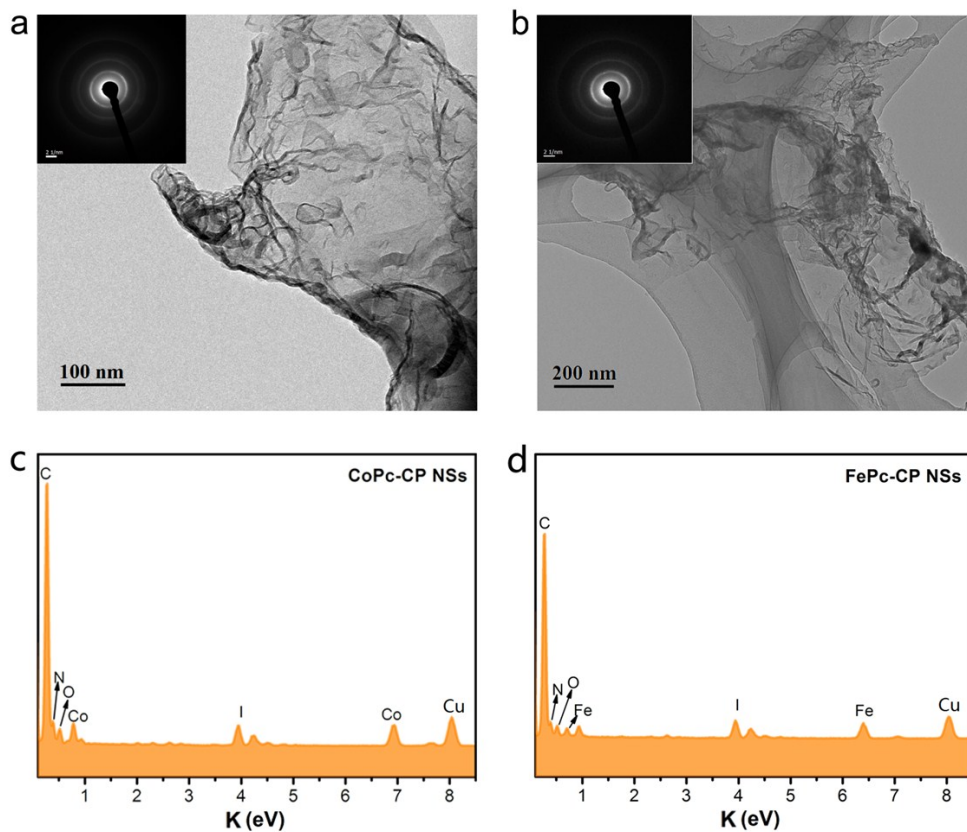
Fig. S8 TEM images and SAED pattern of (a) CoPc-CP NSs and (b) FePc-CP NSs. EDS of (c) CoPc-CP NSs and (d) FePc-CP NSs.
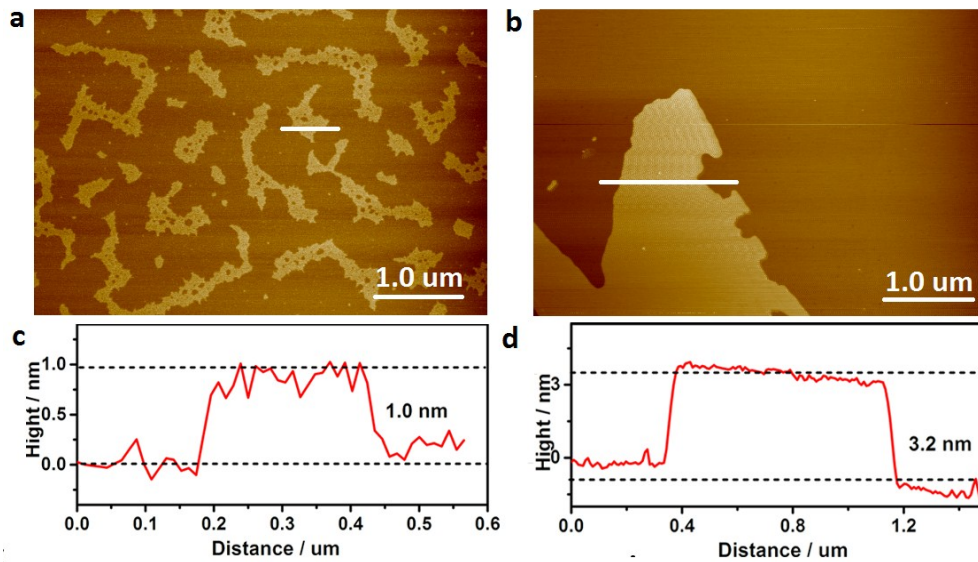
Fig. S9 AFM image and the corresponding height profiles of (a, c) CoPc-CP NSs and (b, d) FePc-CP NSs.
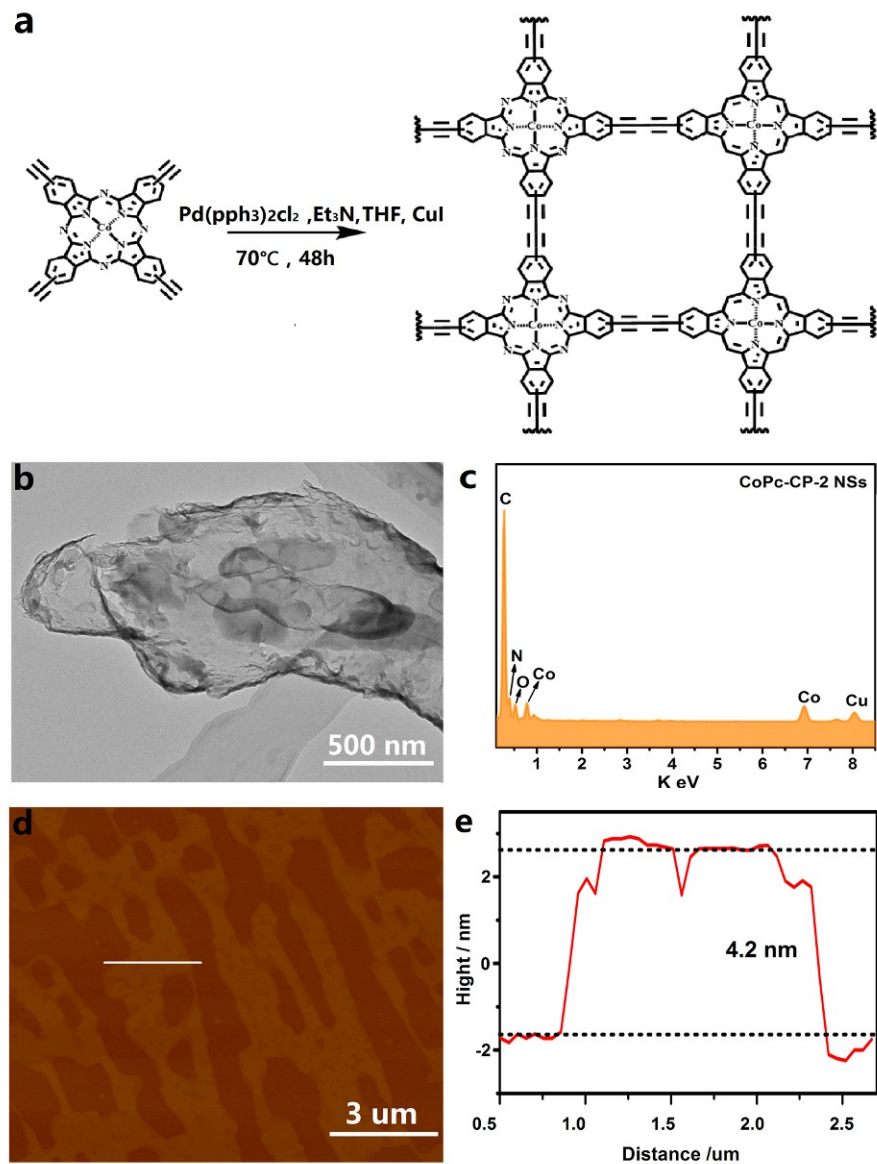
Fig. S10 (a) Schematic diagram for the synthesis of the CoPc-CP-2. The TEM (b) and EDS (c) of CoPc-CP-2 NSs. AFM image (d) and the corresponding height profiles (e) of CoPc-CP-2 NSs.
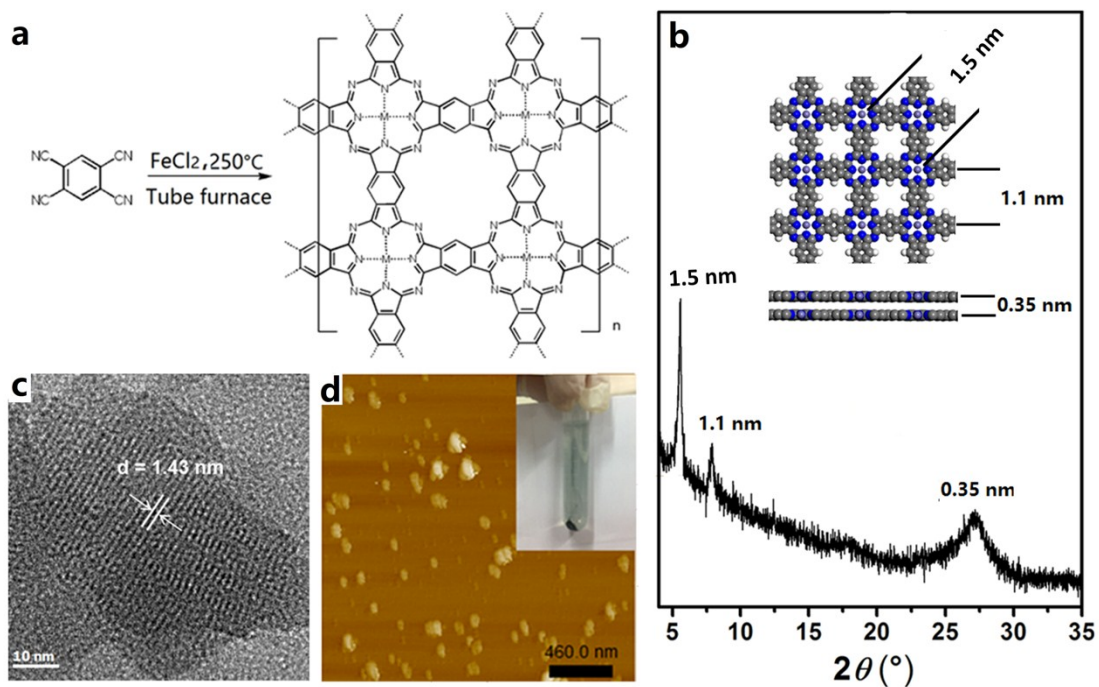
Fig. S11 (a) Schematic diagram for the synthesis of the FePc-CP-3. (b) PXRD patterns of FePc-CP-3. Inset shows the top and side views of the structures of FePc-CP-3. (c) The HRTEM of FePc-CP-3. (d) AFM image of FePc-CP-3 after ultrasonic exfoliation for 8 h in ethanol. Inset: Photograph of the FePc-CP-3 after ultrasonic exfoliation.
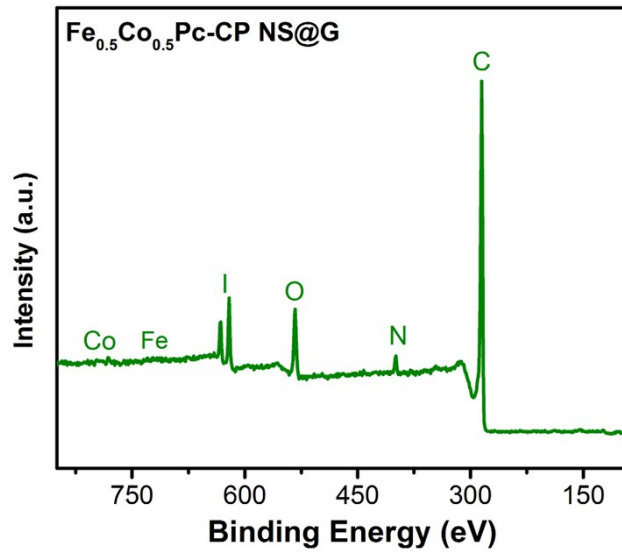
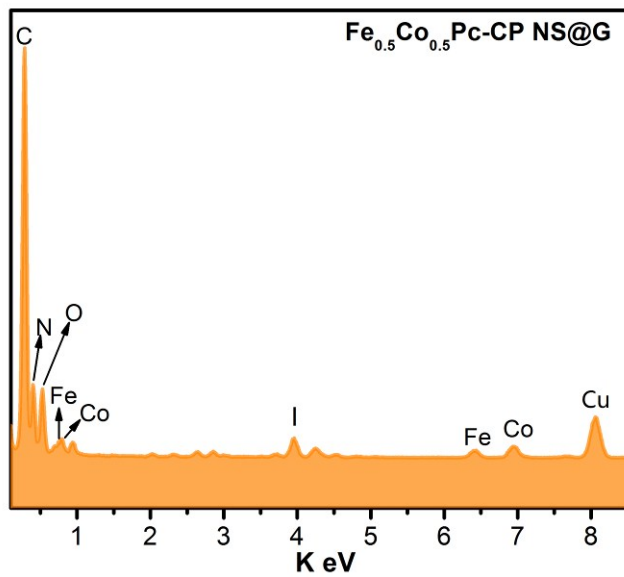**Fig. S12** XPS overall spectra of $Fe_{0.5}Co_{0.5}Pc$-CP NS@G

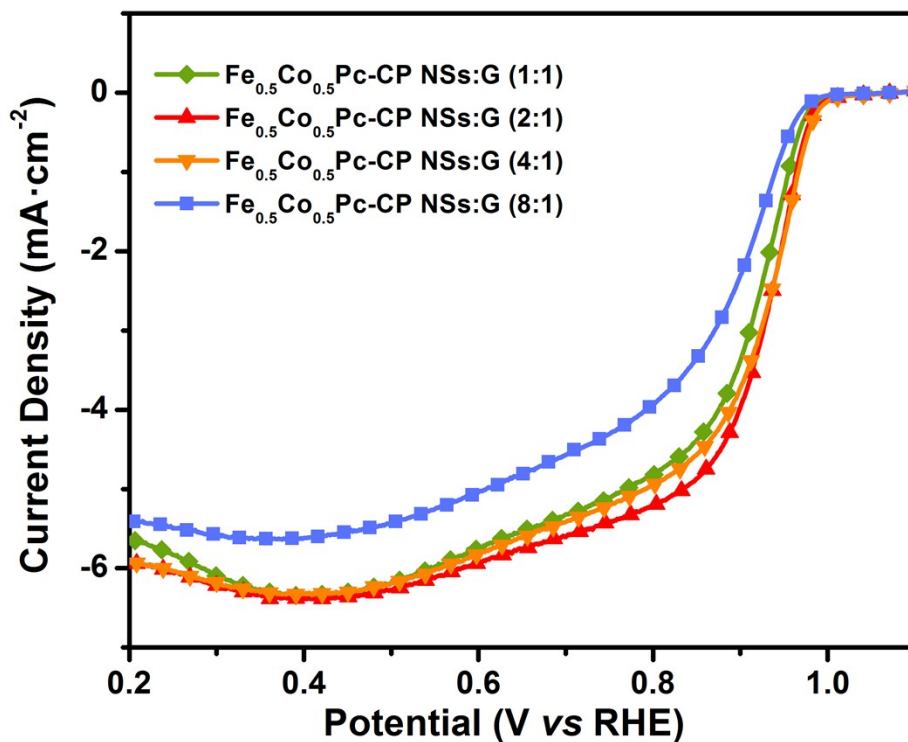**Fig. S13** Energy dispersive spectroscopy (EDS) results of the Fe$_{0.5}$Co$_{0.5}$Pc-CP NS@G.

Fig. S14. LSV curves of $Fe_{0.5}Co_{0.5}Pc$-CP NS@G wirh the ratio between $Fe_{0.5}Co_{0.5}Pc$-CP NS and G of 1:1, 2:1, 4:1, and 8:1 (denoted as $Fe_{0.5}Co_{0.5}Pc$-CP NS@G (1:1), $Fe_{0.5}Co_{0.5}Pc$-CP NS@G (2:1), $Fe_{0.5}Co_{0.5}Pc$-CP NS@G (4:1), and $Fe_{0.5}Co_{0.5}Pc$-CP NS@G (8:1), respectively) at the scan rate of 10 mV s^{-1} with the rotation speed of 1600 rpm in O_2-saturated 0.1 M KOH solution.
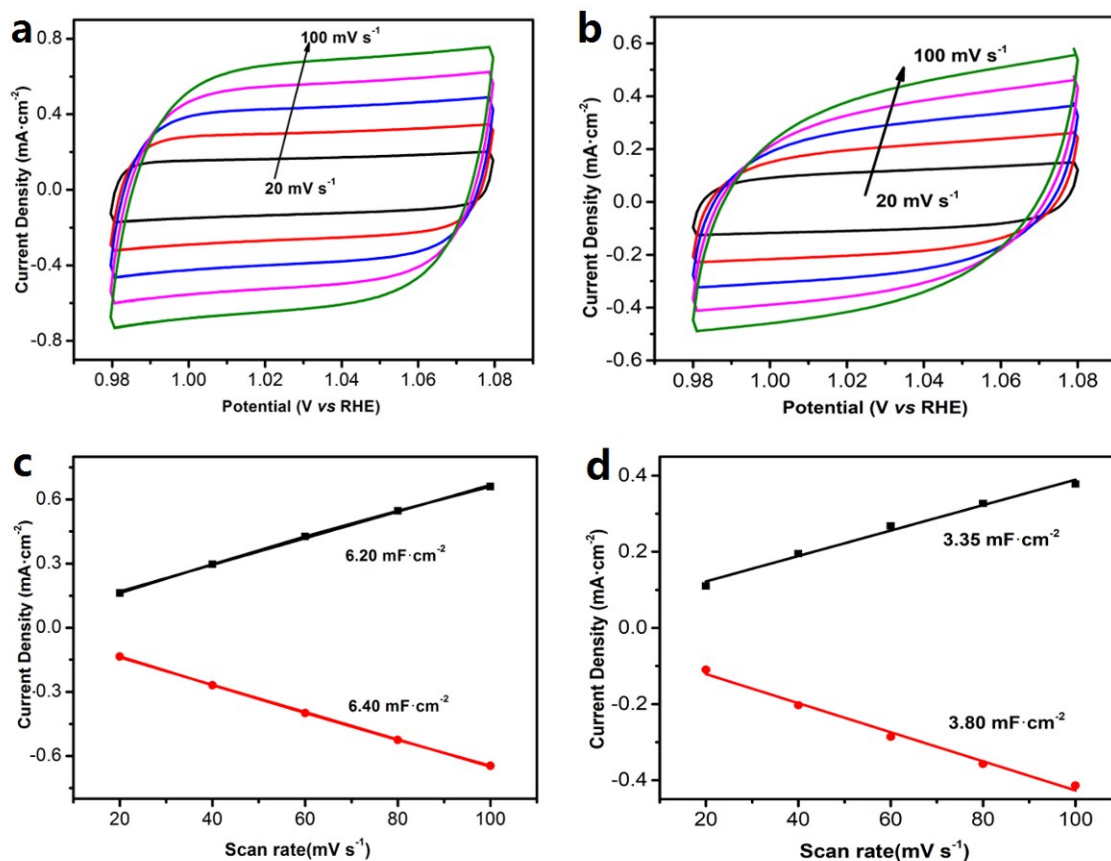
Fig. S15 (a)(b) CV conducted at potential from 0.98 V to 1.08 V *vs* RHE at scan rates of 20 mV s^{-1}, 40 mV s^{-1}, 60 mV s^{-1}, 80 mV s^{-1}, and 100 mV s^{-1} in 0.1 M KOH. (c)(d) The current densities of anode and cathode measured at 1.02 V *vs* RHE with different scan rates. (a)(c) and (b)(d) are Fe$_{0.5}$Co$_{0.5}$Pc-CP NS@G and Fe$_{0.5}$Co$_{0.5}$Pc-CP&G. respectively.

To study the electrochemically active surface area (ECSA) of Fe$_{0.5}$Co$_{0.5}$Pc-CP NS@G and Fe$_{0.5}$Co$_{0.5}$Pc-CP&G. we conducted the CV cycles at different scan rates during the potential from 0.98V to 1.08V *vs* RHE in 0.1 M KOH, where there is no Faradic current. At last, the ECSA was estimated from the as obtained double-layer capacitance (C$_{dl}$). According to C$_{dl}$ is constant, it can be calculated as:

$$C_{dl} = Q/U = (dQ/dt)/(dU/dt) = j/r \tag{8}$$

Q is the quantity of electric charge per unit area,

U is the voltage,

j is the current density and

r is the scan rate

From Eq(1), the C_{dl} is the slope of $j \sim r$, which can be obtained by the Fig. S15c and S15d. The average Cdl of $Fe_{0.5}Co_{0.5}Pc$-CP NS@G and $Fe_{0.5}Co_{0.5}Pc$-CP&G are 6.3 mF/cm^2, and 3.6 mF/cm^2, respectively. The ECSA can be calculated as:

$$ECSA = C_{dl}/C_s \tag{9}$$

C_s is the specific capacitance value for a flat standard with 1 cm^2 of real surface area. The general value for C_s is between 20 µF/cm^2 and 60 µF/cm^2. Here we use 40 µF/cm^2 as the average value (*Nat. Commun.* **2015**, *6*, 8668). Thus the ECSA for $Fe_{0.5}Co_{0.5}Pc$-CP NS@G and $Fe_{0.5}Co_{0.5}Pc$-CP&G can be obtained as 159 cm^2 and 90 cm^2. respectively.
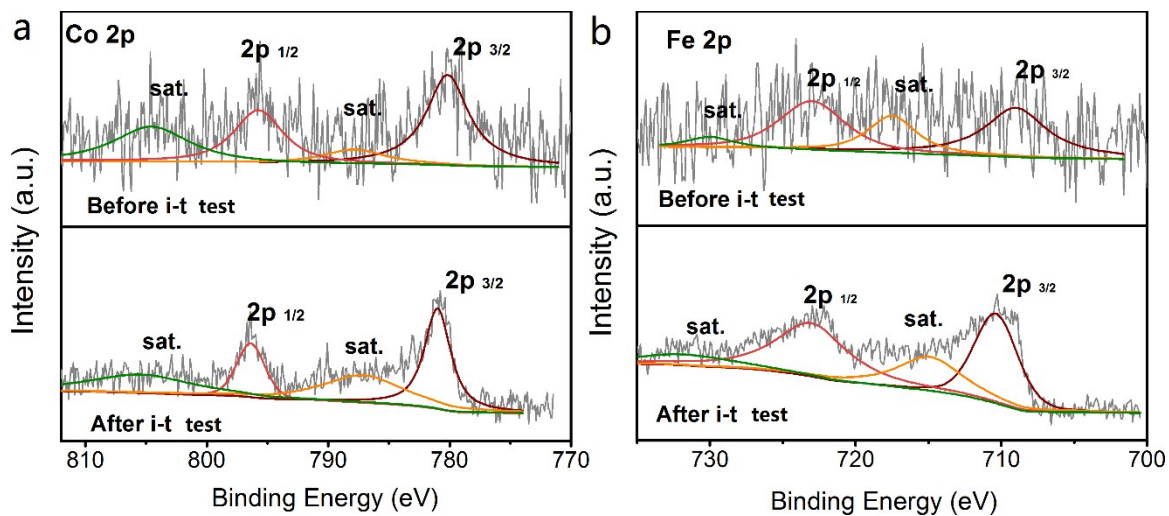
Fig. S16. XPS high resolution (a) Co 2p and (b) Fe 2p spectra of $Fe_{0.5}Co_{0.5}Pc$-CP NS@G before and after i-t test.
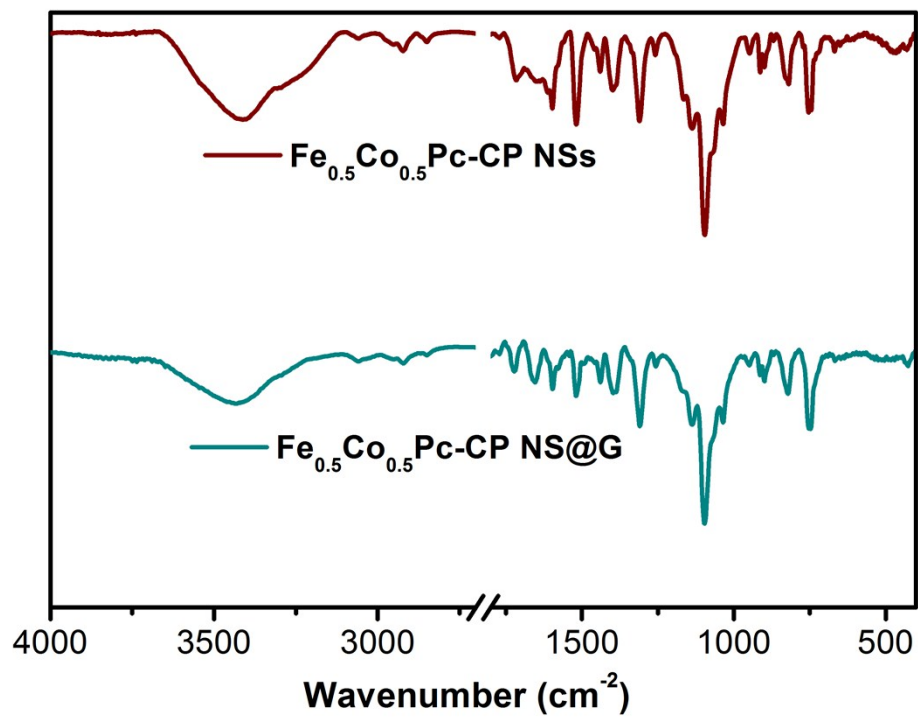
Fig. S17. FT-IR spectra of $Fe_{0.5}Co_{0.5}Pc$-CP NSs and $Fe_{0.5}Co_{0.5}Pc$-CP NS@G in the region of 400-4000 cm^{-1}.
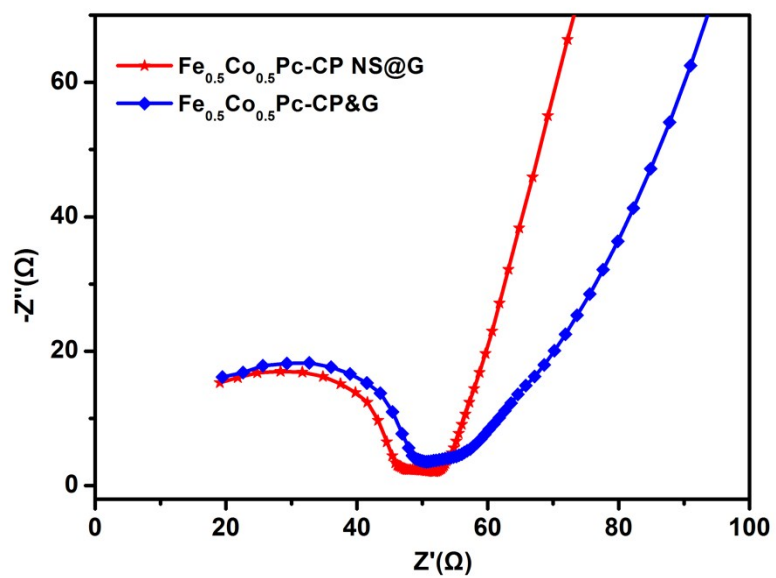
Fig. S18. Impedance curve of $Fe_{0.5}Co_{0.5}Pc$-CP NS@G and $Fe_{0.5}Co_{0.5}Pc$-CP&G.
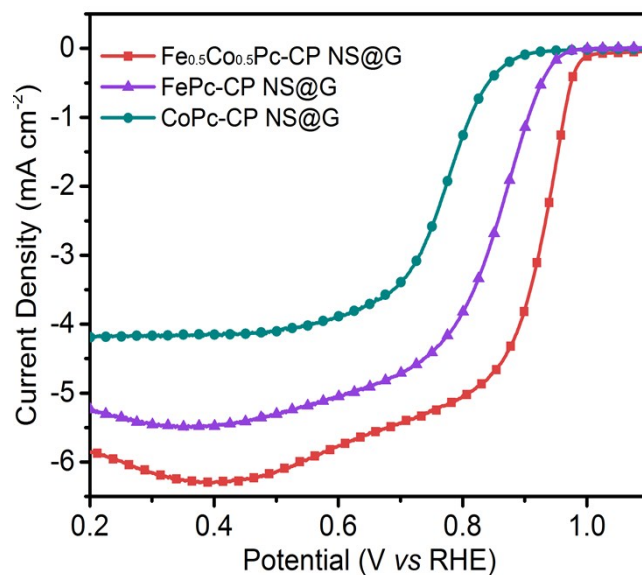
Fig. S19. LSV curves of $Fe_{0.5}Co_{0.5}Pc$-CP NS@G, FePc-CP NS@G, and CoPc-CP NS@G wirh the ratio between MPc-CP NS and G of 2:1 at the scan rate of 10 mV s^{-1} with the rotation speed of 1600 rpm in O_2-saturated 0.1 M KOH solution. It can be seen that the $Fe_{0.5}Co_{0.5}Pc$-CP NS@G exhibits much better ORR catalytic activity than the two single metal counterparts, suggesting the synergetic effect between the proximate Fe and Co ions in the conjugated network. This is well in line with the result found for the corresponding bulk materials as revealed in ref. S1

Fig. S20. (a) XPS overall spectra of $Fe_{0.5}Co_{0.5}Pc$-CP NS@G before and after being washed by EDTA-Na. (b) LSV curves of $Fe_{0.5}Co_{0.5}Pc$-CP N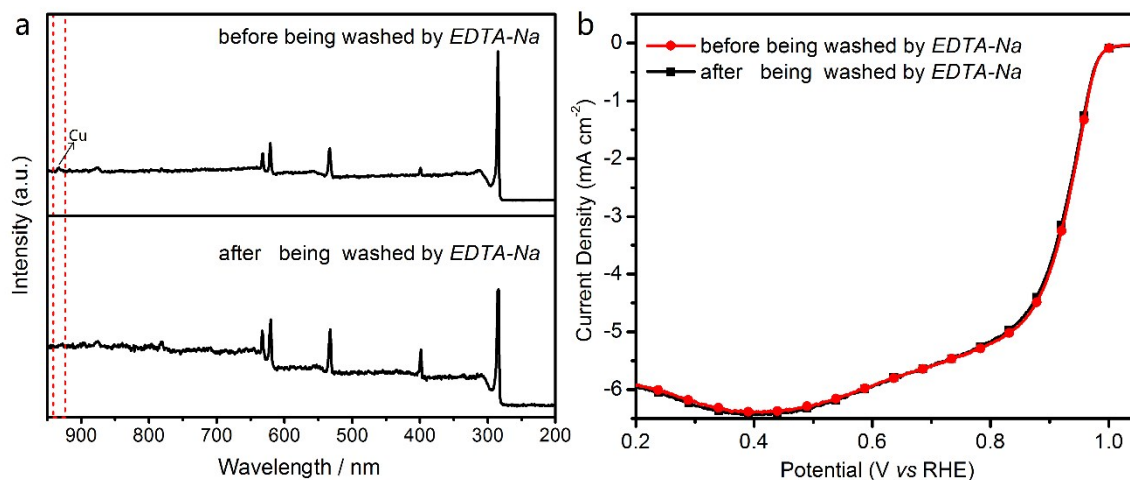S@G before and after being washed by EDTA-Na at the scan rate of 10 mV s^{-1} with the rotation speed of 1600 rpm in O_2-saturated 0.1 M KOH solution.

In order to exclude the contribution to the catalytic activity from the Cu deposits, the $Fe_{0.5}Co_{0.5}Pc$-CP NS@G was also washed by EDTA-Na solution, and the content of Cu in the washed $Fe_{0.5}Co_{0.5}Pc$-CP NS@G was tested by XPS. As shown in Fig. S20a in the revised ESI and given below, the signals for Cu almost disappear, proving that the Cu residue was removed. Nevertheless, the ORR properties of the $Fe_{0.5}Co_{0.5}Pc$-CP NS@G before and after being washed by EDTA-Na are just the same (see Fig. S20b), which excludes the contribution to the catalytic activity from the Cu deposits.

Table S1. Comparison of ORR electrocatalytic performance of various nonprecious metal catalysts in 0.1 M KOH.

Catalyst	Rotation and scan rate	Onset potential (V *vs* RHE)	Half-wave potential (V *vs* RHE)	Reference
$Fe_{0.5}Co_{0.5}$Pc-CP NS@G	1600 rpm and 10 mV s^{-1}	1.006 V	0.927	This work
$Fe_{0.5}Co_{0.5}$Pc-CP&G	1600 rpm and 10 mV s^{-1}	0.954	0.855	This work
D-AC@2Mn-4Co	1600 rpm and 10 mV s^{-1}	0.883 V	0.803	[S10]
NCNTFs	1600 rpm and 10 mV s^{-1}	0.97	0.87	[S11]
Co–C_3N_4/CNT	1600 rpm and 10 mV s^{-1}	0.9	—	[S12]
Fe3C@N-CNT	1600 rpm and 10 mV s^{-1}	—	0.85	[S13]
$Co_3FeS_{1.5}(OH)_6$	1600 rpm and 10 mV s^{-1}	0.867	0.721	[S14]
Fe–N-CNTAs-5-900	1600 rpm and 10 mV s^{-1}	0.97	0.88	[S15]
FeCl1N4/CNS	1600 rpm and 10 mV s^{-1}	—	0.921	[S16]
(Fe,Mn)-N-C	1600 rpm and 10 mV s^{-1}	0.98	0.900	[S17]
Fe-ISAs/CN	1600 rpm and 10 mV s^{-1}	—	0.9	[S18]
GL-Fe/Fe_5C_2/NG-800	1600 rpm and 10 mV s^{-1}	0.98	0.86	[S19]
CNT/PC	1600 rpm and 10 mV s^{-1}	—	0.88	[S20]
pCNT@Fe1.5@GL	1600 rpm and 5 mV s^{-1}	0.936	0.883	[S21]
Co SAs/N-C(900)	1600 rpm and 10 mV s^{-1}	0.982	0.881	[S22]
S,N-Fe/N/C-CNT	1600 rpm and 10 mV s^{-1}	—	0.85	[S23]
Co@MCM	1600 rpm and 10 mV s^{-1}	0.95 V	0.86	[S24]

References

[S1] W. Liu, Y. Hou, H. Pan, W. Liu, D. Qi, K. Wang, J. Jiang and X. Yao, *J. Mater. Chem. A,* 2018, **6**, 8349-8357.

[S2] Y. Liang, Y. Li, H. Wang, J. Zhou, J. Wang, T. Regier and H. Dai, *Nat. Mater.,* 2011, **10**, 780-786.

[S3] Y. Liang, H. Wang, J. Zhou, Y. Li, J. Wang, T. Regier and H. Dai, *J. Am. Chem. Soc.,* 2012, **134**, 3517-3523.

[S4] S. Wang, D. Yu, L. Dai, D. Chang and J.-B. Baek, *ACS Nano,* 2011, **5**, 6202-6209.

[S5] Y. Zhu, W. Zhou, Z. Chen, Y. Chen, C. Su, O. M. Tadé and Z. Shao, *Angew. Chem., Int. Ed.,* 2015, **54**, 3897-3901.

[S6] P. Perdew, K. Burke and M. Ernzerhof, *Phys. Rev. Lett.,* 1996, **77**, 3865-3868.

[S7] P. Hay and W. Wadt, *J. Chem. Phys.,* 1985, **82**, 270-283.

[S8] J. Binkley, J. Pople and W. Hehre, *J. Am. Chem. Soc.,* 1980, **102**, 939-947.

[S9] M. J. Frisch, et al. Gaussian 09, Revision D.01. Wallingford, CT: Gaussian Inc.; 2013.

[S10] X. Yan, Y. Jia, J. Chen, Z. Zhu and X. Yao, *Adv. Mater.,* 2016, **28**, 8771-8778.

[S11] B. Xia, Y. Yan, N. Li, H. Wu, X. Lou and X. Wang, *Nature Energy,* 2016, **1**, 8.

[S12] Y. Zheng, Y. Jiao, Y. Zhu, Q. Cai, A. Vasileff, L. Li, Y. Han, Y. Chen and S. Qiao, *J. Am. Chem. Soc.,* 2017, **139**, 3336-3339.

[S13] B. Guan, L. Yu and X. Lou, *Energy Environ. Sci.,* 2016, **9**, 3092-3096.

[S14] H. Wang, C. Tang, B. Wang, B. Li and Q. Zhang, *Adv. Mater.,* 2017, **29**, 1702327.

[S15] C. Zhu, S. Fu, J. Song, Q. Shi, D. Su, M. Engelhard, X. Li, D. Xiao, D. Li, L. Esteez, D. Du and Y. Lin, *Small,* 2017, **13**, 1603407.

[S16] Y. Han, Y. Wang, R. Xu, W. Chen, L. Zheng, A. Han, Y. Zhu, J. Zhang, H. Zhang, J. Luo, C. Chen, Q. Peng, D. Wang and Y. Li, *Energy Environ. Sci.,* 2018, **11**, 2348-2352.

[S17] N. Sahraie, U. Kramm, J. Steinberg, Y. Zhang, A. Thomas, T. Reier, J. P. Paraknowitsch and P. Strasser, *Nat. Commun.,* 2015, **6**, 8618.

[S18] Y. Chen, S. Ji, Y. Wang, J. Dong, W. Chen, Z. Li, R. Shen, L. Zheng, Z. Zhuang, D. Wang and Y. Li, *Angew. Chem., Int. Ed.,* 2017, **56**, 6937-6941.

[S19] X. Tian, L. Wang, B. Chi, Y. Xu, S. Zaman, K. Qi, H. Liu, S. Liao and B. Xia, *ACS Catal.,* 2018, **8**, 8970-8975.

[S20] Y. J. Sa, D. J. Seo, J. Woo, J. T. Lim, J. Y. Cheon, S. Y. Yang, J. M. Lee, D. Kang, T. J. Shin, H. S. Shin, H. Y. Jeong, C. S. Kim, M. G. Kim, T. Y. Kim and S. H. Joo, *J. Am. Chem. Soc.,* 2016, **138**, 15046-15056.

[S21] S. H. Ahn, X. W. Yu and A. Manthiram, *Adv. Mater.,* 2017, **29**, 1606534.

[S22] P. Yin, T. Yao, Y. Wu, L. Zheng, Y. Lin, W. Liu, H. Ju, J. Zhu, X. Hong, Z. Deng, G. Zhou, S. Wei and Y. Li, *Angew. Chem., Int. Ed.,* 2016, **55**, 10800-10805.

[S23] P. Chen, T. Zhou, L. Xing, K. Xu, Y. Tong, H. Xie, L. Zhang, W. Yan, W. Chu, C. Wu and Y. Xie, *Angew. Chem., Int. Ed.,* 2017, **56**, 610-614.

[S24] H. Zhang, W. Zhou, T. Chen, B. Guan, Z. Li and X. Lou, *Energy Environ. Sci.,* 2018, **11**, 1980-1984.